Correspondence and
requests for materials
should be addressed to
A.F.G. (agoncharov@
carnegiescience.edu)

Vibrational, electronic and structural properties of wurtzite GaAs nanowires under hydrostatic pressure

Wei Zhou[1], Xiao-Jia Chen[1,2], Jian-Bo Zhang[3], Xin-Hua Li[1], Yu-Qi Wang[1] & Alexander F. Goncharov[1,4]

[1]Key Laboratory of Materials Physics and Center for Energy Matter in Extreme Environments, Institute of Solid State Physics, Chinese Academy of Sciences, Hefei 230031, China, [2]Center for High Pressure Science and Technology Advanced Research, Shanghai 201203, China, [3]Department of Physics, South China University of Technology, Guangzhou 510640, China, [4]Geophysical Laboratory, Carnegie Institution of Washington, Washington D.C. 20015, U.S.A.

The structural, vibrational, and electronic properties of GaAs nanowires have been studied in the metastable wurtzite phase via Resonant Raman spectroscopy and synchrotron X-ray diffraction measurements in diamond anvil cells under hydrostatic conditions between 0 and 23 GPa. The direct band gap E_0 and the crystal field split-off gap $E_0 + \Delta$ of wurtzite GaAs increase with pressure and their values become close to those of zinc-blende GaAs at 5 GPa, while being reported slightly larger at lower pressures. Above 21 GPa, a complete structural transition from the wurtzite to an orthorhombic phase is observed in both Raman and X-ray diffraction experiments.

The existence of GaAs in the form of nano particles and nanowires (NW) modifies the traditional electronic structures and thus provides new opportunities for the semiconducting industry including optoelectronics, photovoltaic and solar cell applications. Recently, an electrically driven GaAs NW light emitting diode was coupled to plasmonic nanostrip waveguides[1]. GaAs NW were also grown on graphite and graphene for potential optoelectronic applications[2]. However, to integrate III–V NW into the low cost silicon solar cells, it is desirable to tune their band gap values above 1.4 eV[3] continuously. Among the present mechanical methods in bandgap adjustment, a remarkable decrease of GaAs/Al$_{0.3}$Ga$_{0.7}$As/GaAs NW bandgap was found under both tensile and compressive stresses, the maximum of which is 290 meV[4]. Recently, the strain induced band gap decrease of mono and bilayer MoS$_2$ was reported[5]. On the contrary, band gap of GaAs is well known to increase with hydrostatic pressure at the rate of 0.1 eV/GPa for both zinc-blende (ZB) phase of bulk GaAs[6–9] and recently investigated ZB GaAs NW[10]. Thus, application of hydrostatic pressure provides an alternative approach to explore and tune optoelectronic properties of GaAs NW and other novel semiconductors needed for applications. Knowledge of the deformation potentials of optoelectronic materials is necessary to design novel materials with optimized properties.

At ambient conditions, bulk GaAs crystallizes only in ZB phase, however GaAs NW and nanoparticles can exist in pure wurtzite (WZ) phase as well as demonstrate coexistence of WZ and ZB phases[11]. WZ and ZB GaAs differ by the stacking sequence of Ga-As bilayers, which results in the Brillouin Zone folding in WZ GaAs, that in turn leads to additional Raman active modes and a modified electronic band structure including a different direct band gap E_0 and three valence band gaps of heavy hole, light hole and crystal field split-off hole Δ states[12–14]. The values of E_0 of WZ GaAs NW were reported to span the range from 1.46 eV[15] to 1.56 eV[16], generally larger than those of ZB GaAs samples reported as 1.42 eV and 1.44 eV[16,17]. However, in some photoluminescence experiments E_0 of WZ GaAs NW was found to be smaller than that of ZB ones[18–20]. The reason of such a discrepancy could be due to the sensitivity of E_0 to slightly different fabrication and experimental conditions, which could result in variable structural parameters. Thus, it is highly desirable to study the stress dependence of the band gap, as this is valuable for both fundamental science and practical applications. Here we use an external hydrostatic pressure to tune the electronic and vibrational properties of WZ GaAs in the form of NW.

Under hydrostatic pressure, bulk ZB GaAs was investigated extensively and its P-T phase diagram has been reported[21]. Recently ZB GaAs NW were studied in a diamond anvil cell up to 21 GPa at 300 K in resonant Raman scattering (RRS) and photoluminescence experiments[10]. Pressure dependent vibrational properties and direct band gap were explored, and a possible phase change above 16 GPa was suggested. However, there is no high

pressure Raman investigation of the WZ phase of GaAs NW so far and their high-pressure structural research is rare. In a synchrotron x-ray diffraction study (XRD)[22], WZ phase of GaAs was obtained on decompression of the simple cubic phase GaAs of 16 atoms down to ambient pressure. Then WZ to orthorhombic (OR) phase transition was observed at 18.7 GPa. Recently, the difficulties in WZ GaAs fabrication have been overcome due to the development of molecular beam epitaxy and metal organic chemical vapor deposition techniques[11,20,23] thus enabling studies of the structural, vibrational, and electronic properties of WZ GaAs nano materials under pressure.

In this work, we report experimental investigations of structural, vibrational, and electronic properties of WZ and ZB GaAs NW by combining RRS and synchrotron XRD techniques at high pressures up to 23 GPa at room temperature. We find that WZ GaAs behaves similarly to ZB GaAs in its relation to structural and vibrational properties. Our RRS measurements of the direct and split-off band gaps of WZ GaAs suggest a slight difference in pressure slopes between WZ and ZB, but the values of the pressure dependencies of the gaps become very close above 5 GPa.

GaAs NW of WZ and ZB phase were fabricated using Au-assisted molecular beam epitaxy method, with an average length of 5 μm and diameter of 150 nm, as detailed previously[24]. A diamond anvil cell was used to generate pressure up to 23 GPa, diamond culet diameter was 300 μm and sample chambers of drilled rhenium gaskets were about 130 μm in diameter and 40 μm of thickness initially. Neon was used as pressure transmitting medium and backscattering geometry was adopted for micro confocal Raman measurements. Pressures were measured by means of ruby fluorescence. We applied the RRS technique to investigate vibrational and electronic structure changes of WZ GaAs NW under pressure. Pressure effects on band gap of WZ GaAs NW are explored by using two different incident lasers of wavelengths of 532 nm and 488 nm. Pressure was increased from near 0 GPa to 21.5 GPa, then it was brought down to ambient pressure.

For synchrotron XRD measurements up to 23.0 GPa, a mixture of WZ and ZB GaAs NW were loaded into the diamond anvil cell, thus making it possible to investigate the WZ and ZB structure evolution with pressure at the same time. In the synchrotron beam line, sector 13 of the Advanced Photon Source of the Argonne National Laboratory (Chicago, United States), the monochromatic signals (λ = 0.3344 Å) were collected by a MAR 355 CCD detector about 300 mm away from the sample. At every pressure point, 25 measurements at different sample positions were taken to confirm data consistency and reduce the effect of preferable orientation. In a separate high-pressure synchrotron experiment, another load of bulk GaAs in ZB phase (bulk WZ GaAs is not readily available as it is metastable) was also measured at the same conditions for a direct comparison with NW samples.
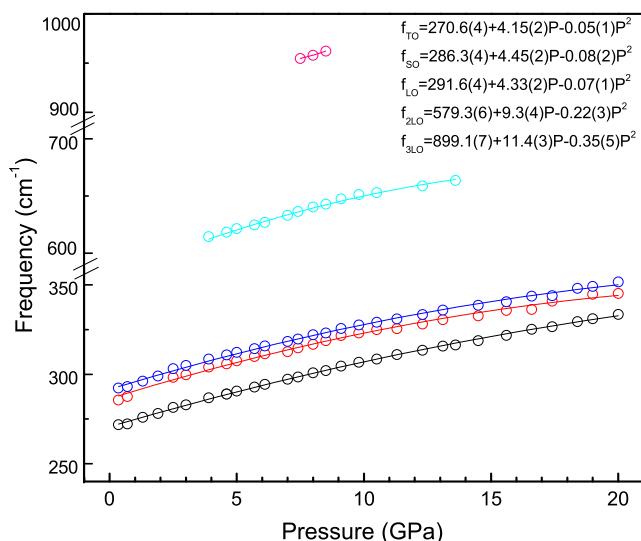
At ambient conditions, Raman spectra of both WZ and ZB GaAs NW show three modes: transverse optical (TO), surface optical (SO) and longitudinal optical (LO) around 270, 285, and 291 cm^{-1}, respectively. The LO modes and their overtones, 2LO and 3LO modes (around 580 cm^{-1} and 870 cm^{-1} at ambient conditions) show an increase in intensity and become comparable or even larger than that of the TO mode in the resonant conditions (due to resonance enhancement via dipole-forbidden Fröhlich electron-phonon interaction[25,26]), when the incident laser energy is close to the band gap. Since the spectra measured with the 488 nm and 532 nm excitation wavelengths are similar, only spectra measured with 532 nm excitation are shown in Fig. 1. At low pressures, the LO mode is weak and it has an asymmetric shape due to the presence of the nearby SO mode of comparable intensity. The band gap increases with pressure resulting in resonance conditions for 532 and 488 nm excitation wavelengths sequentially. This is manifested in an increase of the LO mode intensity with respect to TO and SO modes. We observed two strong 2LO resonances at 5.7 GPa and
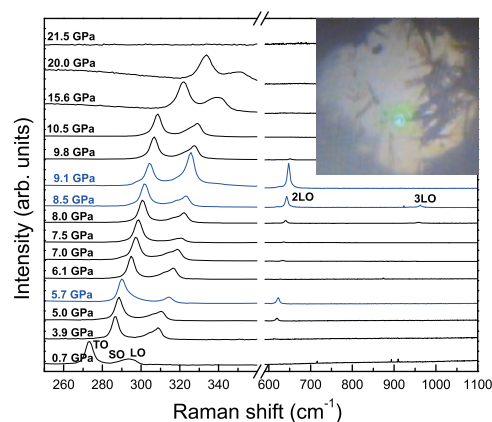
Figure 1 | Pressure dependence of Raman spectra of WZ GaAs NW up to 21.5 GPa, all spectra are scaled and shifted vertically for clarity. The laser wavelength is 532 nm except for the spectrum at 21.5 GPa, which was excited by 488 nm laser line. The spectra shown in blue at 5.7 GPa and 9.1 GPa indicate two strong resonances of 2LO, while that at 8.5 GPa shows the strongest 3LO resonance. Insert: a microphotograph of WZ GaAs NW in diamond anvil cell high pressure cavity, a blue spot is the 488 nm laser spot (about 4 μm in diameter), which was kept at the same localized region of a NW bundle for both 532 nm and 488 nm laser lines during Raman experiments.

9.1 GPa, as well as a clear 3LO resonance at 8.5 GPa as shown in Fig. 1. These occur when the pressure modified band gaps (including direct band gap E_0 and band gap split-off Δ) are close to the incident laser energy. No Raman modes were observed at pressures larger than 21 GPa (Fig. 1).

In Fig. 2, we present Raman mode frequencies for the 532 nm laser as a function of pressures. Raman shifts measured using 488 nm wavelengths agree well with those of 532 nm within experimental error bars, which shows good consistency for our measurements. The linear coefficients as well as the Grüneisen parameters γ of 4 Raman

$f_{TO} = 270.6(4) + 4.15(2)P - 0.05(1)P^2$
$f_{SO} = 286.3(4) + 4.45(2)P - 0.08(2)P^2$
$f_{LO} = 291.6(4) + 4.33(2)P - 0.07(1)P^2$
$f_{2LO} = 579.3(6) + 9.3(4)P - 0.22(3)P^2$
$f_{3LO} = 899.1(7) + 11.4(3)P - 0.35(5)P^2$

Figure 2 | Pressure dependence of the experimental Raman frequencies of WZ NW measured with the 532 nm excitation wavelength (the results for the 488 nm excitation are consistent yielding similar Grüneisen parameters presented in Table I). The symbols are the data; the lines are the least square fits through the data. For the fitting to the 2nd order polynomials, the frequencies are in the unit of cm^{-1} and pressure is in GPa.

Table I | The mode Grüneisen parameters at ambient pressure of WZ and ZB bulk and NW GaAs materials derived from the measured phonon frequencies and the equation of state using the formula $\gamma = \dfrac{B_0}{\omega_0}\left(\dfrac{\partial \omega_0}{\partial P}\right)_{P=0}$, where $B_0 = 74.66$ GPa[27]. The data labeled as 532 nm and 488 nm are from this work

Samples	γ_{TO}	γ_{SO}	γ_{LO}	γ_{2LO}	References
WZ NWs	1.15(5)	1.16(6)	1.1(6)	1.2(8)	532 nm
WZ NWs	1.11(5)	1.14(5)	1.03(5)	1.15(8)	488 nm
ZB NWs	1.31(4)	1.22(4)	1.17(3)	1.26(9)	Zardo et al.[10]
ZB bulk	1.39	NA	1.23	NA	Weinstein et al.[27]

modes (TO, SO, LO and 2LO) determined by $\gamma = \dfrac{B_0}{\omega_0}\left(\dfrac{\partial \omega_0}{\partial P}\right)_{P=0}$, where the isothermal bulk modulus $B_0 = 74.66$ GPa[27]. The values of the Grüneisen parameters for our WZ sample are somewhat smaller than those for ZB GaAs NW[10] and bulk ZB[27] as presented in Table I. This small deviation may be due to a difference in the data representation in this work and Refs. 10, 27. Moreover, in our calculations we have used the literature value of the bulk modulus of ZB GaAs, which may be slightly different of that for WZ GaAs. Our x-ray diffraction measurements (see below) are not sufficiently accurate to quantify this difference; however, they broadly agree with the literature data for ZB GaAs. The proximity of the Grüneisen parameters of ZB and WZ GaAs shows the similarity of vibrational properties of WZ and ZB GaAs, as expected given their closely related structures. In Ref. 21, pressure dependent Raman modes of bulk ZB were measured up to 20 GPa, and the phase transition from ZB to OR phase was suggested at 21 GPa for bulk ZB GaAs. In Ref. 10, no distinguishable Raman spectra of ZB NW were collected above 16 GPa, which might be due to inhomogeneous stress conditions in the solid methanol-ethanol pressure medium. Our data present the first observation of Raman spectra of WZ GaAs NW under pressure up to the structural transition to the OR phase at 21 GPa as determined by our synchrotron XRD experiment described below.

To explore the pressure dependent band gaps of WZ GaAs NW, 532 nm (2.33 eV) and 488 nm (2.54 eV) incident lasers were used in high pressure RRS experiments. When pressure tuned band gaps are close to the laser light energies, "forbidden" LO and even higher order LO modes can be observed. In our experiments, we observed and analyzed not only the resonant enhancement of TO and LO intensities as recently reported for ZB GaAs NW[10] and WZ InAs NW[28] under pressure, but also the relative intensities of LO and 2LO modes with respect to the increase of the TO mode at resonances, as shown in Fig. 1. In Fig. 3 (a) and (b), the integrated intensities of LO and 2LO modes were normalized to that of the TO mode as in the previous RRS study of GaAs NW using varying incident laser energies and temperatures[13,16]. The resonances of the 1LO and 2LO modes almost coincide because of the small energies of phonons (approximately 0.04 eV for 1LO). The normalized 1LO and 2LO intensities have two resonance pressures, which are at 5.7 GPa and 9.1 GPa for 532 nm, and at 7.0 GPa and 11.8 GPa for 488 nm lasers. The normalized 2LO intensities show stronger resonances than 1LO ones at 9.1 GPa and 11.8 GPa, which shows sharp outgoing resonances (see also Ref. 10). The resonances that occur at larger pressures are due to the proximity of incident laser energy to the direct band gap E_0. From two resonances at 9.1 GPa for the 532 nm laser and 11.8 GPa for the 488 nm laser (red circles in Fig. 3 (c)) as well as the literature data of 1.52 eV at 0 GPa[13], the pressure slope of E_0 is determined to be 0.087(3) eV/GPa (Fig. 3 (c)), which is close to values of ZB GaAs: 0.1 eV/GPa for bulk ZB GaAs[6] and 0.105 eV/GPa of GaAs ZB NW[10]. Moreover, the proximity of pressure slopes for ZB and WZ GaAs can be even closer if we adopt that $E_0(P)$ of WZ GaAs has a curvature as it has been found for ZB
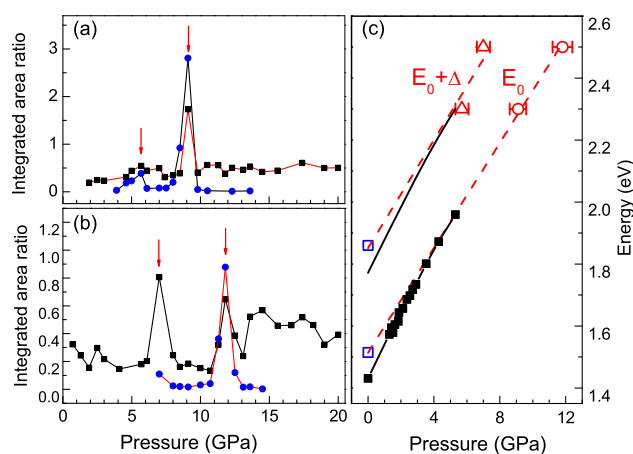

Figure 3 | Pressure dependence of the integrated area ratio of 1LO over TO (black squares) and 2LO over TO (blue circles) of WZ GaAs NW for (a) 532 nm laser and (b) 488 nm laser. Red arrows indicate resonance pressures for E_0 and $E_0 + \Delta$. (c) red symbols with error bars are RRS data of this work, blue symbols at 0 GPa are data from[13]; red dashed lines as linear fitting of three data points (two of this work and one of literature[13]) yielding the pressure slopes of E_0 and $E_0 + \Delta$ as 0.087 (3) eV/GPa and 0.084 (11) eV/GPa, respectively. Filled black squares are data of direct band gap of ZB GaAs NW[10], with its polynomial fitting in a black solid line. The pressure dependence of the split-off band gap is approximated by another black solid line above, assuming the pressure independent $\Delta_{SO} = 0.34$ eV of WZ GaAs NW.

GaAs[10]. Two weaker resonances that occur at 5.7 GPa for the 532 nm laser and 7.0 GPa for the 488 nm laser (red triangles in Fig. 3. (c)) can be ascribed to the resonant condition of $E_L = E_0 + \Delta + E_{phonon}$, where Δ is the lowest valence band gap due to crystal field split-off hole state. With the value of 1.86 eV at 0 GPa and room temperature[13], the fitting to a linear function gives the pressure slope of $E_0 + \Delta$ as 0.084 (11) eV/GPa, which is about the same as that of E_0 within the experimental error bars. Thus Δ is likely to be weakly pressure dependent. This agrees well with the assumption of Ref. 10 of the pressure independent $\Delta_{SO} = 0.34$ eV (Fig. 3 (c)). One can see that the band gaps of WZ GaAs behave similarly with pressure but the values of the slopes are slightly larger than those of ZB GaAs below 5 GPa. Our high pressure RRS experiment determines the pressure slopes of E_0 and $E_0 + \Delta$ of WZ GaAs NW separately for the first time, which provides an effective approach to tune electronic structure. Also, a combination of hydrostatic pressure and the RRS technique can be extended to probe and tune band gaps of other novel materials such as few layered graphene and MoS2, whose strain induced band gap decrease was recently reported to be similar to GaAs NW[4,5].

To confirm the pressure induced phase change from our Raman observations as well as to determine the structural behaviors of WZ GaAs NW in comparison with the behavior of ZB GaAs ones, we have investigated a mixture of WZ and ZB GaAs NW by synchrotron XRD technique at room temperature. The presence of WZ phase is clearly detectable by observations of the scattering angles of 5.5 and 6.3 degrees corresponding to (100) and (110) reflections of WZ phase GaAs (Fig. 4), which are absent in ZB phase. At 19.2 GPa, new diffraction peaks of OR phase appear while those of WZ and ZB decrease sharply in intensity signaling a phase transformation as shown in Fig. 4. WZ and ZB phases coexist with the OR phase at 19–21 GPa. At 22 GPa and above, only OR phase can be observed, which implies the phase transition from WZ and ZB to OR is completed in a very narrow pressure range. We believe that this sharpness is due to the use of neon as a pressure transmitting medium, which remains almost hydrostatic in the pressure range of WZ to OR phase
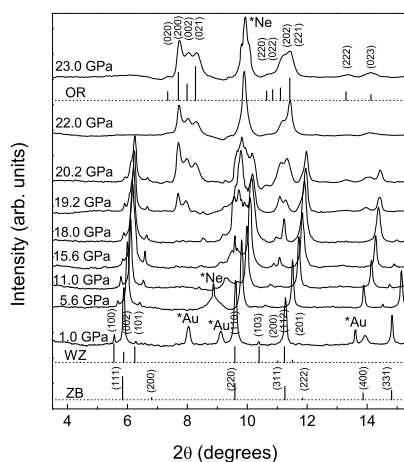
Figure 4 | XRD patterns of WZ and ZB NW mixture at various pressures, ticks of WZ and ZB phases are assigned at 1.0 GPa and ticks of OR phase (Cmcm, Ref.22) at 23 GPa; their positions and lengths indicate diffraction peak positions and relative intensities from simulations of the software PowderCell (Ref. 29). Neon peak around 10 degrees at 23 GPa is marked by asterisk.

transition. Our measurements demonstrate that WZ GaAs NW show the same phase transition to OR phase as ZB GaAs NW and bulk ZB studied before[21]. Our Raman and XRD data are consistent in that they both indicate phase changes in the same pressure range. While Raman spectra do not show any measurable activity of the metallic OR phase, XRD clearly identifies the high pressure phase as the same one, that is observed for the transformation of ZB GaAs. In the depressurization process, there were still no Raman modes which would reappear suggesting the "irreversible" WZ and ZB to OR phase transition. This result is also consistent with the disappearance of ZB GaAs NW Raman modes in the depressurization process from 20.8 GPa[10].

In summary, we have performed RRS and synchrotron XRD experiments of WZ GaAs NW under pressure up to 23 GPa at room temperature. Before phase changing to OR structure around 21 GPa, WZ GaAs NW are found to have similar vibrational properties and direct band gap behaviors as those of ZB bulk and NW. We determined the pressure dependence of the E_0 direct band gap of WZ GaAs NW to be linear with the slope of 0.087 eV/GPa, which is slightly smaller than that of ZB GaAs. The crystal field splitting of WZ GaAs NW is observed to be weakly pressure dependent, consistent with the previous assumption of the pressure independence of Δ_{SO} of ZB GaAs. The similarity of vibrational and structural properties of WZ and ZB GaAs NW can be an advantage to incorporating two types of GaAs NWs into one device and even into one single NW; at the same time their band gap difference can be used to realize different electronic functions by fine tuning approaches including but not limited to pressure. It is hoped that our experimental findings will stimulate further development of theoretical research as well as potential applications.

1. Pengyu, F. et al. An Electrically-Driven GaAs Nanowire Surface Plasmon Source. *Nano Lett.* **12**, 4943–4947, doi:10.1021/nl302521v (2012).
2. Munshi, A. M. et al. Vertically Aligned GaAs Nanowires on Graphite and Few-Layer Graphene: Generic Model and Epitaxial Growth. *Nano Lett.* **12**, 4570–4576, doi:10.1021/nl3018115 (2012).
3. Holm, J. V. et al. Surface-passivated GaAsP single-nanowire solar cells exceeding 10% efficiency grown on silicon. *Nat. Commun.* **4**, 1498, doi:10.1038/ncomms2510 (2013).
4. Signorello, G., Karg, S., Björk, M. T., Gotsmann, B. & Riel, H. Tuning the Light Emission from GaAs Nanowires over 290 meV with Uniaxial Strain. *Nano Lett.* **13**, 917–924, doi:10.1021/nl303694c (2013).
5. Conley, H. J. et al. Bandgap Engineering of Strained Monolayer and Bilayer MoS_2. *Nano Lett.* **13**, 3626–3630, doi:10.1021/nl4014748 (2013).
6. Wei, S. H. & Zunger, A. Predicted band-gap pressure coefficients of all diamond and zinc-blende semiconductors: Chemical trends. *Phys. Rev. B* **60**, 5404, doi:http://dx.doi.org/10.1103/PhysRevB.60.5404 (1999).
7. Paul, W. The effect of pressure on the properties of germanium and silicon. *J. PHYS. CHEM. SOLIDS* **8**, 196–204, doi:http://dx.doi.org/10.1016/0022-3697(59)90315-4 (1959).
8. Welber, B., Cardona, M., Kim, C. K. & Rodriguez, S. Dependence of the direct energy gap of GaAs on hydrostatic pressure. *Phys. Rev. B* **12**, 5729, doi: http://dx.doi.org/10.1103/PhysRevB.12.5729 (1975).
9. Goni, A. R., Strössner, K., Syassen, K. & Cardona, M. Pressure dependence of direct and indirect optical absorption in GaAs. *Phys. Rev. B* **36**, 1581, doi:http://dx.doi.org/10.1103/PhysRevB.36.1581 (1987).
10. Zardo, I. et al. Pressure Tuning of the Optical Properties of GaAs Nanowires. *ACS Nano.* **6**, 3284–3291, doi:10.1021/nn300228u (2012).
11. Spirkoska, D. et al. Structural and optical properties of high quality zinc-blende/wurtzite GaAs nanowire heterostructures. *Phys. Rev. B* **80**, 245325, doi: http://dx.doi.org/10.1103/PhysRevB.80.245325 (2009).
12. Ketterer, B., Heiss, M., Uccelli, E., Arbiol, J. & Morral, A. F. i. Untangling the electronic band structure of wurtzite GaAs nanowires by resonant Raman spectroscopy. *ACS Nano.* **5**, 7585–7592, doi:10.1021/nn202585j (2011).
13. Ketterer, B. et al. Determination of the band gap and the split-off band in wurtzite GaAs using Raman and photoluminescence excitation spectroscopy. *Phys. Rev.B* **83**, 125307, doi:http://dx.doi.org/10.1103/PhysRevB.83.125307 (2011).
14. Zardo, I. et al. Raman spectroscopy of wurtzite and zinc-blende GaAs nanowires: Polarization dependence, selection rules, and strain effects. *Phys. Rev. B* **80**, 245324, doi: http://dx.doi.org/10.1103/PhysRevB.80.245324 (2009).
15. Kusch, P. et al. Band gap of wurtzite GaAs: A resonant Raman study. *Phys. Rev. B* **86**, 075317, doi: http://dx.doi.org/10.1103/PhysRevB.86.075317 (2012).
16. Peng, W., Jabeen, F., Jusserand, B., Harmand, J. C. & Bernard, M. Conduction band structure in wurtzite GaAs nanowires: A resonant Raman scattering study. *Appl. Phys. Lett.* **100**, 073102, doi:http://dx.doi.org/10.1063/1.3684837 (2012).
17. Brewster, M., Schimek, O., Reich, S. & Gradecak, S. Exciton-phonon coupling in individual GaAs nanowires studied using resonant Raman spectroscopy. *Phys. Rev. B* **80**, 201314, doi:http://dx.doi.org/10.1103/PhysRevB.80.201314 (2009).
18. Moewe, M., Chuang, L. C., Crankshaw, S., Chase, C. & Chang-Hasnain, C. Atomically sharp catalyst-free wurtzite GaAs/AlGaAs nanoneedles grown on silicon. *Appl. Phys. Lett.* **93**, 023116, doi:http://dx.doi.org/10.1063/1.2949315 (2008).
19. Martelli, F. et al. Photoluminescence of Mn-catalyzed GaAs nanowires grown by molecular beam epitaxy. *Nanotechnology* **18**, 125603, doi:10.1088/0957-4484/18/12/125603 (2007).
20. Hoang, T. B. et al. Observation of free exciton photoluminescence emission from single wurtzite GaAs nanowires. *Appl. Phys. Lett.* **94**, 133105, doi:10.1063/1.3104853 (2009).
21. Besson, J. M. et al. High-pressure phase transition and phase diagram of gallium arsenide. *Phys. Rev. B* **44**, 4214, doi: 10.1103/PhysRevB.44.4214 (1991).
22. McMahon, M. I. & Nelmes, R. J. Observation of a Wurtzite Form of Gallium Arsenide. *Phys. Rev. Lett.* **95**, 215505, doi: http://dx.doi.org/10.1103/PhysRevLett.95.215505 (2005).
23. Song, Y. et al. Growth and Characterization of Radial pn Junction Gaas Nanowire by MOCVD. *Adv. Mater. Res.* **457-458**, 165–169, doi:10.4028/www.scientific.net/AMR.457-458.165 (2012).
24. Li, X. Morphology and crystal structure control of GaAs nanowires grown by Au-assisted MBE with solid As_4 source. *J. Crys. Grow.* **324**, 82–87, doi:http://dx.doi.org/10.1016/j.jcrysgro.2011.04.004 (2011).
25. Trommer, R. & Cardona, M. Resonant Raman scattering in GaAs. *Phys. Rev. B* **17**, 1865, doi: http://dx.doi.org/10.1103/PhysRevB.17.1865 (1978).
26. Kauschke, W., Cardona, M. & Bauser, E. Resonant Raman scattering by LO phonons in $Al_xGa_{1-x}As$ (x < 0.1): Alloying and interference effects. *Phys. Rev. B* **35**, 8030, doi: http://dx.doi.org/10.1103/PhysRevB.35.8030 (1987).
27. Weinstein, B. A. & Zallen, R. Pressure-Raman Effects in Covalent and Molecular Solids. In *Light Scattering in Solids IV*; Springer: Heidelberg, doi: 10.1007/3-540-11942-6_26 (1984).
28. Zardo, I. et al. $E_1(A)$ Electronic Band Gap in Wurtzite InAs Nanowires Studied by Resonant Raman Scattering. *Nano Lett.* **13**, 3011–3016, doi:10.1021/nl304528j (2013).
29. Kraus, W. & Nolze, G. POWDER CELL - a program for the representation and manipulation of crystal structures and calculation of the resulting X-ray powder patterns. *J. Appl. Cryst.* **29**, 301–303, doi:10.1107/S0021889895014920 (1996).

Acknowledgments

Author contributions

Additional information